J Biochem Technol (2025) 16(1): 24-33
https://doi.org/10.51847/U7jSlxe2f8
ISSN: 0974-2328

# Plant-Mediated Green Synthesis of Iron Oxide Nanoparticles Using *Catharanthus roseus* and Assessment of Antibacterial Properties

**John Babu Dulla*, Lasya Priya Kanchibotla, Chinna Venkateswarulu Tirupati, Sumalatha Boddu, Vidya Prabhakar Kodali**

Received: 09 January 2025 / Received in revised form: 18 March 2025, Accepted: 18 March 2025, Published online: 25 March 2025

## Abstract

Nanoparticle production has attracted attention because of its unique properties and broad variety of applications in environmental cleanup, materials research, and medicine. Due to its magnetic qualities, biocompatibility, and potential for application in biomedicine, iron oxide nanoparticles ($Fe_3O_4$) are highly prized among them. Traditional synthesis methods, however, often involve toxic chemicals and harsh conditions. This study explores a green synthesis approach using leaf extract of *Catharanthus roseus* (periwinkle), an alkaloidal and bioactive compound-rich medicinal plant that acts as a natural maintaining and decreasing agent. $Fe_3O_4$ nanoparticles were synthesized under varying conditions of extract concentration, temperature, and pH to optimize the process. X-ray diffraction (XRD), UV-Vis spectroscopy, scanning electron microscopy (SEM), and Fourier-transform infrared spectroscopy (FTIR) were employed for characterization, confirming the production of unique, functionalized nanoparticles. The agar well dispersion technique was used to evaluate the produced $Fe_3O_4$ nanoparticles' antibacterial efficacy against Escherichia coli and Staphylococcus aureus. Significant antibacterial activity was shown by the results, and all tested strains showed distinct zones of inhibition. These results demonstrate the potential of $Fe_3O_4$ nanoparticles mediated by *C.roseus* as environmentally benign antibacterial agents that may be used in environmental and biomedical settings. This green synthesis method provides a sustainable substitute for the traditional manufacturing of nanoparticles.

**John Babu Dulla*, Lasya Priya Kanchibotla, Chinna Venkateswarulu Tirupati**
Department of Biotechnology, Vignan's Foundation for Science, Technology and Research, Vadlamudi, Guntur District, Andhra Pradesh, India.

**Sumalatha Boddu**
Department of Chemical Engineering, Vignan's Foundation for Science, Technology and Research, Vadlamudi, Guntur District, Andhra Pradesh, India.

**Vidya Prabhakar Kodali**
Department of Biotechnology, Vikrama Simhapuri University, Nellore District, Andhra Pradesh, India.

***E-mail:** johnbabud77@gmail.com

**Keywords:** Green synthesis, Iron oxide nanoparticles, *Catharanthus roseus*, Antibacterial activity

## Introduction

The precise manipulation of materials at the atomic or molecular scale, usually between 1 and 100 nanometers, is known as nanotechnology. Materials at this nanoscale have different physical, chemical, and biological characteristics from their bulk counterparts because to their high surface area-to-volume ratio and quantum effects (Aljerf & Nadra, 2019; Seifi & Masoum, 2020). Iron oxide nanoparticles ($Fe_3O_4$) are one type of nanomaterial that has garnered a lot of interest due to their potential uses in electronics, biology, catalysis, and environmental remediation (Rahmani *et al*., 2020). These nanoparticles are especially notable for their magnetic behaviour (Asfahani, 2022; Kariri *et al*., 2022; Nguyen *et al*., 2022a, 2022b; Üzüm *et al*., 2022), biocompatibility (Gouyau *et al*., 2021), and low toxicity, making them perfect for applications like medication administration, magnetic resonance imaging (MRI), environmental sensing, and antibacterial therapies (Yassin *et al*., 2024). $Fe_3O_4$ nanoparticles can have their size and surface chemistry finely controlled, increasing their adaptability in a variety of fields (Ma *et al*., 2013). Because they are superparamagnetic—magnetized only when an external magnetic field is present and loses its magnetization when it is removed—they are particularly helpful for targeted medication delivery, magnetic separation, and hyperthermia-based cancer treatment (İlhan *et al*., 2022; Yoong *et al*., 2022; İlaslan *et al*., 2023; Alamu *et al*., 2024). Owing to their high biocompatibility, $Fe_3O_4$ nanoparticles are well-suited for therapeutic and diagnostic applications (Alexeree *et al*., 2024).

$Fe_3O_4$ nanoparticles have strong bactericidal effects in the context of antibacterial activity, mainly via mechanisms including reactive oxygen species (ROS) production that damages bacterial membranes, proteins, and DNA (Zhan *et al*., 2023). This makes them a viable substitute for traditional antibiotics, especially when it comes to addressing the growing problem of antibiotic resistance (Dadfar *et al*., 2019). However, traditional nanoparticle synthesis methods often rely on hazardous chemicals like sodium borohydride or hydrazine and demand extreme reaction conditions, posing serious environmental and health hazards (Pirsaheb *et al*., 2024).

On the other hand, using biological molecules or plant extracts as reduction and limitation agents, green synthesis has become a viable and ecologically safe substitute. This environmentally benign method enables scalable manufacturing, lowers energy use, and does away with the need for hazardous chemicals. (Ahmed *et al*., 2016). Additionally, plant-mediated synthesis often imparts surface functional groups beneficial for biomedical applications due to their inherent bioactivity (Singh *et al*., 2018). Alkaloids, flavonoids, and polyphenols are among the many biomolecules found in plants, which serve as efficient natural reducers for nanoparticle formation (Potbhare *et al*., 2019).

*Catharanthus roseus* (periwinkle), a widely used medicinal plant, is particularly suitable for green synthesis due to its high alkaloid content and broad pharmacological activity (Abdel-Hadi & Abdel-Fattah, 2022; Kauser *et al*., 2022; Nakagawa *et al*., 2022; Soboleva *et al*., 2022; Xuan *et al*., 2022), including antioxidant, antibacterial, and anticancer properties (Gajalakshmi *et al*., 2013). It is indigenous to Madagascar and has long been utilized to treat diabetes, hypertension, and cancer (Figueroa-Valverde *et al*., 2024; Kwatra *et al*., 2024). Vincristine, vinblastine, and ajmalicine are among the bioactive substances found in the plant that have strong reducing properties (Pham *et al*., 2020). In addition to its therapeutic value, *C. roseus* provides a wealth of antioxidants and secondary metabolites that can aid in the manufacturing of nanoparticles of iron oxide with regulated functionality and shape (Gavamukulya *et al*., 2014). This green synthesis method is ecologically friendly in addition to being affordable and scalable.

Given the escalating global challenge of antibiotic resistance, the antibacterial characteristics of $Fe_3O_4$ nanoparticles are particularly significant. Research has shown that these nanoparticles are effective against both Gram-positive and Gram-negative bacteria (Sirelkhatim *et al*., 2015), primarily through ROS production, membrane disruption, and interaction with intracellular biomolecules, resulting in the killing of microorganisms (Abo-zeid *et al*., 2020). Moreover, $Fe_3O_4$ nanoparticles can function as effective drug transporters, increasing the effectiveness of antibiotics while reducing their negative impacts (Vitta *et al*., 2020). The combination of plant-derived biomolecules with $Fe_3O_4$ nanoparticles may also produce synergistic antibacterial effects, offering innovative strategies to combat multidrug-resistant pathogens (Patra & Baek, 2014).

## Materials and Methods

*Reagents and Chemicals*

Ferric nitrate, sodium hydroxide, and other analytical-grade reagents were procured from Merck (India). Fresh *C.roseus* leaves were collected from the university's botanical garden for use in nanoparticle synthesis.

*Preparation of Plant Extract*

Using phytochemicals found in plants as natural reduction and stabilization agents, green synthesis provides an environmentally responsible and sustainable method of producing nanoparticles. Because *C.roseus* has a rich phytochemical profile that includes alkaloids, flavonoids, and phenolic substances that aid in the bioreduction of metal ions, it was chosen for this investigation.

Healthy, fully grown *C.roseus* leaves were selected, properly cleaned under running water, and cleaned to take out dust and other surface contaminants with condensed water. For the purpose of eliminating moisture, the cleaned leaves were oven-dried at 50 to 60°C, then finely powdered using a mortar and pestle. 10 g of the powdered leaves were boiled in 100 mL of distilled water for an hour at 70°C in a water bath to extract the bioactive ingredients. Whatman No. 1 filter paper was used to filter the mixture once it had cooled to room temperature. Iron oxide nanoparticles were produced using the resultant clear aqueous extract as a biogenic cap and decreasing agent (Venkateswarlu *et al*., 2014).

*Green Synthesis of Iron Oxide Nanoparticles*

Iron oxide nanoparticles ($Fe_3O_4$) were made using extract from *C.roseus* as a green reducing agent. Ten grams of ferric nitrate [$Fe(NO_3)_3$] were dissolved in one hundred milliliters of condensed water to create the precursor solution. The solution was then added dropwise while being continuously swirled into a sterile 300 mL conical flask containing the plant extract.

Subsequently, 8 g of sodium hydroxide (NaOH) was gradually introduced into the reaction mixture to adjust the pH and initiate nanoparticle formation. The reaction was continuously stirred and let to continue for sixty minutes at ambient temperature. As the $Fe^{2+}$ ions were reduced and iron oxide nanoparticles were formed, the color gradually changed from yellow to dark brown and then reddish-brown. To separate the nanoparticles, the solution was transferred to 50 mL centrifuge tubes and spun at 10,000 rpm for 25 minutes at 25°C (Nnadozie & Ajibade, 2020). In order to eliminate any remaining phytochemicals and contaminants, the pellet was repeatedly cleaned with ethanol after the supernatant was disposed of. For further characterization and biological assessment, the pure nanoparticles were oven-dried and kept in airtight containers.

*Assessment of Antimicrobial Activity*

The antibacterial qualities of the generated $Fe_3O_4$ nanoparticles were evaluated utilizing the disc diffusion method. In 100 milliliters of distilled water, 2 grams of agar-agar and 2.1 grams of Mueller Hinton medium were dissolved to create a nutritional medium. In aseptic circumstances, the medium was placed onto sterile Petri plates after being sanitized and allowed to harden.

To create a homogenous solution for testing, 1 g of the dried nanoparticles was combined with 1 mL of distilled water and vigorously stirred. Staphylococcus aureus (Gram-positive) and Escherichia coli (Gram-negative) standardized cultures were injected onto sterile Petri plates using a sterile glass spreader to guarantee uniform distribution. After being properly positioned onto the infected agar plates, sterile filter paper discs were impregnated with the nanoparticle solution. To facilitate microbial growth and nanoparticle diffusion, at 37°C, the plates had been incubating for 24 hours (Buarki *et al*., 2022). In order to assess the $Fe_3O_4$ nanoparticles' antibacterial efficacy, during incubation,

measurements were made of the zones of inhibition encompassing the discs.

*Characterization Techniques*

A variety of sophisticated characterization methods were used to verify the effective production of $Fe_3O_4$ nanoparticles and examine their physicochemical characteristics.

*Fourier Transform Infrared Spectroscopy (FTIR)*

The functional groups connected to the produced $Fe_3O_4$ nanoparticles were identified using the FTIR method. In order to remove any remaining organic molecules and unreacted iron ions, the 100 mL suspension of nanoparticles was concentrated at 8000 rpm for 10 minutes. The final pellet was thoroughly purified by washing it three times with 10 mL of sterile deionized water. The dried nanoparticle powder was then finely ground and mixed with approximately 100 mg of potassium bromide (KBr) to form translucent pellets for FTIR analysis (Chinnasamy *et al*., 2024). Spectra were recorded using a Bruker 6700 FTIR spectrometer across the range of 400–4000 $cm^{-1}$. The distinctive absorption bands revealed details about surface-bound functional groups involved in stabilization and validated the existence of Fe–O linkages.

*Scanning Electron Microscopy (SEM)*

SEM was employed to examine the $Fe_3O_4$ nanoparticles' surface appearance and structural properties. To improve conductivity, a little portion of the dry sample was placed onto an aluminum stub coated with carbon and thinly coated with gold using sputtering. The sample was then examined under a high-resolution SEM, enabling visualization of nanoparticle shape, size, and distribution.

*Energy Dispersive X-ray Spectroscopy (EDS)*

EDS examination verified the $Fe_3O_4$nanoparticles' elemental composition. An aliquot of the nanoparticle dispersion (10 microliters) was drop-cast onto a carbon stub and allowed for curing at room temperature. Spectra were captured using a JEOL JSM 6360 SEM connected to an EDX detector at an accelerating voltage of 20 kV. Elemental mapping using pseudo-colored 2D images revealed the spatial distribution of elements, verifying that iron and oxygen are the two main components (Moorthi *et al*., 2015).

*X-ray Diffraction (XRD)*

To ascertain the crystalline structure and calculate the average crystallite size of the $FeO_4$ nanoparticles, XRD examination was carried out. A nickel monochromator and a Rigaku MiniFlex diffractometer running at 40 kV and 30 mA with CuKα radiation (λ = 0.154 nm) were used to get the measurements. A 2θ range of 20° to 80° was used to capture the diffraction patterns in order to identify characteristic peaks that matched the crystal planes of $Fe_3O_4$ (Buarki *et al*., 2022). The Debye-Scherrer equation was used to determine the average crystallite size, confirming the particles' nanoscale crystalline nature.

## Results and Discussion

*Energy Dispersive X-ray Spectroscopy (EDS) of $Fe_3O_4$ nanoparticles*

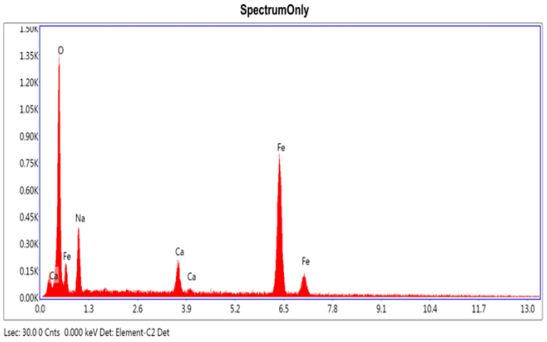


**Figure 1.** Energy Dispersive X-ray Spectroscopy (EDS) Spectrum confirms the presence of iron (Fe) along with oxygen (O), sodium (Na), and calcium (Ca), indicating successful formation of $Fe_3O_4$

The elemental composition analysis via EDS presented in **Figure 1** confirmed the successful synthesis of iron oxide nanoparticles, with iron and oxygen identified as the predominant constituents. A high iron content (48.82 wt%) highlights iron as the core structural element of the nanoparticles, while the substantial oxygen presence supports the formation of an iron oxide phase, consistent with $Fe_2O_3$ or $Fe_3O_4$. The presence of sodium in notable quantities is attributed to the use of sodium hydroxide (NaOH) during synthesis for pH modulation and particle stabilization. A minor calcium signal likely originates from trace minerals inherent in the *C.roseus* extract.

The relatively low standard error associated with iron (2.83%) and oxygen (7.59%) reflects the precision and reliability of the measurements, reinforcing the compositional integrity of the synthesized nanoparticles. The EDS findings further substantiate the success of the green synthesis approach, with the elemental profile aligning well with the anticipated Fe–O framework. Additionally, the detection of trace bioelements suggests phytochemical capping or surface functionalization derived from the plant extract. These results affirm the potential of the synthesized nanoparticles for antimicrobial applications, as validated by subsequent biological assays.

*Scanning Electron Microscopy (SEM) of $Fe_3O_4$ Nanoparticles*

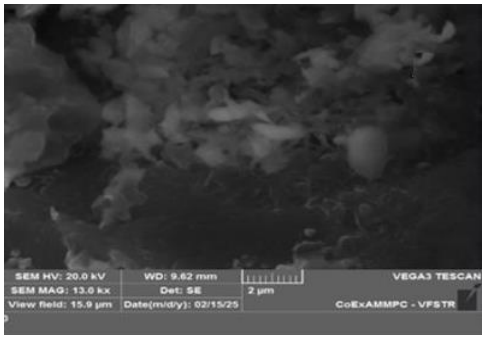


a)

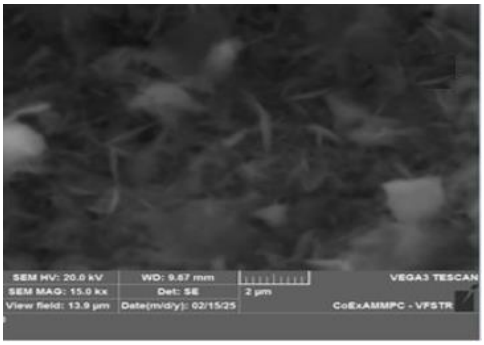


b)

**Figure 2.** SEM image of green synthesized iron oxide nanoparticles a) Surface showing densely aggregated and fine nanostructures embedded in a bioorganic matrix, b) Surface showing rod- and needle-like nanostructures distributed

The SEM analysis of the green-synthesized iron oxide nanoparticles, performed at magnifications ranging from 10.0 kx to 33.0 kx under an accelerating voltage of 20 kV, and presented in **Figure 2** revealed distinct morphological features characteristic of plant-mediated nanoparticle synthesis. At lower magnifications (10.0–15.0 kx), the nanoparticles appeared as aggregated clusters, likely resulting from the inherent magnetic interactions between individual iron oxide particles. The clustering effect may also be influenced by surface-bound phytochemicals derived from *C.roseus* that makes natural stabilization and cap agents.

The micrographs displayed relatively uniform particle size and shape, indicating effective control over the nucleation and growth process during synthesis (Alharith *et al*., 2023; Maneea *et al*., 2023; Maskurova *et al*., 2023; Akhmedov *et al*., 2024; Shaykhaeva *et al*., 2024). The reducing and stabilizing qualities of the bioactive chemicals in the plant extract are responsible for this homogeneity. The observed shape confirms the synthetic material's functional integrity and is in line with other research on biosynthesized iron oxide nanoparticles. In general, the SEM findings support the iron oxide nanoparticles' effective green production, exhibiting structural characteristics like controlled size (Alhazmi *et al*., 2022; Almohmmadi *et al*., 2022; Almuhanna *et al*., 2022; Alqurashi *et al*., 2022; Alsayed *et al*., 2022), shape, and aggregation behaviour that are conducive to enhanced antimicrobial activity.

*FTIR of $Fe_3O_4$ Nanoparticles*

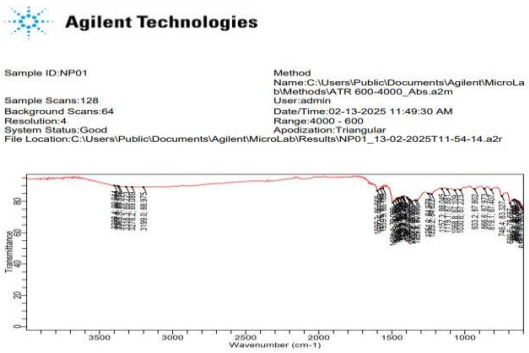


**Figure 3.** FTIR analysis of green generated iron oxide nanoparticles made with extract from *C.roseus*.

**Table 1.** Analysis of the FTIR spectra peak of green-produced iron oxide nanoparticles utilizing extract from *C.roseus*

| Peak Number | Wavenumber ($cm^{-1}$) | Intensity |
|---|---|---|
| **1** | 612.21524 | 75.78304 |
| **2** | 627.59051 | 79.10820 |
| **3** | 637.84069 | 80.07331 |
| **4** | 650.42045 | 80.55821 |
| **5** | 659.27288 | 81.08366 |
| **6** | 669.05714 | 80.55775 |
| **7** | 690.48933 | 78.68722 |
| **8** | 746.39940 | 83.32662 |
| **9** | 819.08249 | 87.40710 |
| **10** | 866.60605 | 87.97283 |
| **11** | 933.23221 | 87.80187 |
| **12** | 1030.60891 | 87.22254 |
| **13** | 1068.81412 | 87.10878 |
| **14** | 1119.13319 | 87.68112 |
| **15** | 1157.33840 | 88.04514 |
| **16** | 1228.15782 | 84.62198 |
| **17** | 1250.98776 | 84.97918 |
| **18** | 1328.79594 | 80.65036 |
| **19** | 1340.90979 | 80.65727 |
| **20** | 1363.27381 | 79.86586 |
| **21** | 1375.38766 | 81.01728 |
| **22** | 1387.96743 | 81.64383 |
| **23** | 1395.88802 | 82.37841 |
| **24** | 1420.11572 | 82.73519 |
| **25** | 1425.24081 | 82.98170 |
| **26** | 1431.29773 | 82.90726 |
| **27** | 1438.28649 | 81.89676 |
| **28** | 1449.00258 | 82.18429 |
| **29** | 1458.32093 | 81.01250 |
| **30** | 1466.24152 | 81.69088 |
| **31** | 1477.88945 | 80.29406 |
| **32** | 1491.40105 | 79.08756 |
| **33** | 1559.89088 | 88.16843 |
| **34** | 1577.59574 | 87.93976 |
| **35** | 1597.16426 | 86.66835 |
| **36** | 3198.98770 | 88.97485 |
| **37** | 3278.19363 | 89.08941 |
| **38** | 3318.26251 | 89.22295 |
| **39** | 3365.32015 | 89.55848 |
| **40** | 3377.43400 | 89.73167 |
| **41** | 3398.40027 | 90.04422 |

Analysis using Fourier-transform infrared spectroscopy (FTIR) confirmed that iron oxide nanoparticles were produced in an environmentally friendly manner. Significant absorption bands in the 400–4000 $cm^{-1}$ range were visible in the FTIR spectrum

**(Figure 3)** and associated peak data **(Table 1)**, suggesting the existence of many functional groups involved in the reduction, stability, and cap of the nanoparticles. Notably, distinct peaks observed at 612.21 $cm^{-1}$, 627.59 $cm^{-1}$, and 650.42 $cm^{-1}$ correspond to Fe–O stretching vibrations, confirming the formation of iron oxide phases such as $Fe_3O_4$ or γ-$Fe_2O_3$.

Broad absorption bands detected between 3198.99 $cm^{-1}$ and 3398.40 $cm^{-1}$ are attributed to O–H stretching vibrations, indicative of hydroxyl groups and polyphenolic compounds present in the *C.roseus* extract. During the production of nanoparticles, these phytochemicals most likely played the dual functions of stabilization and reduction agents.

Other absorption peaks in the range of 1559.89 to 1597.16 $cm^{-1}$ indicate the presence of amide groups, which are most likely the result of proteins or enzymes in the plant extract, which contribute to nanoparticle stabilization through electrostatic interactions. Bands between 1030.61 $cm^{-1}$ and 1387.97 $cm^{-1}$ are indicative of C–O and C–H bending vibrations, which adds more evidence that organic functional groups are involved in the green synthesis method.

All things considered, the FTIR findings provide compelling evidence of the biogenic synthesis of iron oxide nanoparticles, highlighting the beneficial role of plant-derived phytochemicals in the formation and stability of nanoparticles. These functional moieties make these nanoparticles an attractive option for biological and environmental applications since they may have robust antibacterial qualities.

*XRD Analysis of $Fe_3O_4$ Nanoparticles*

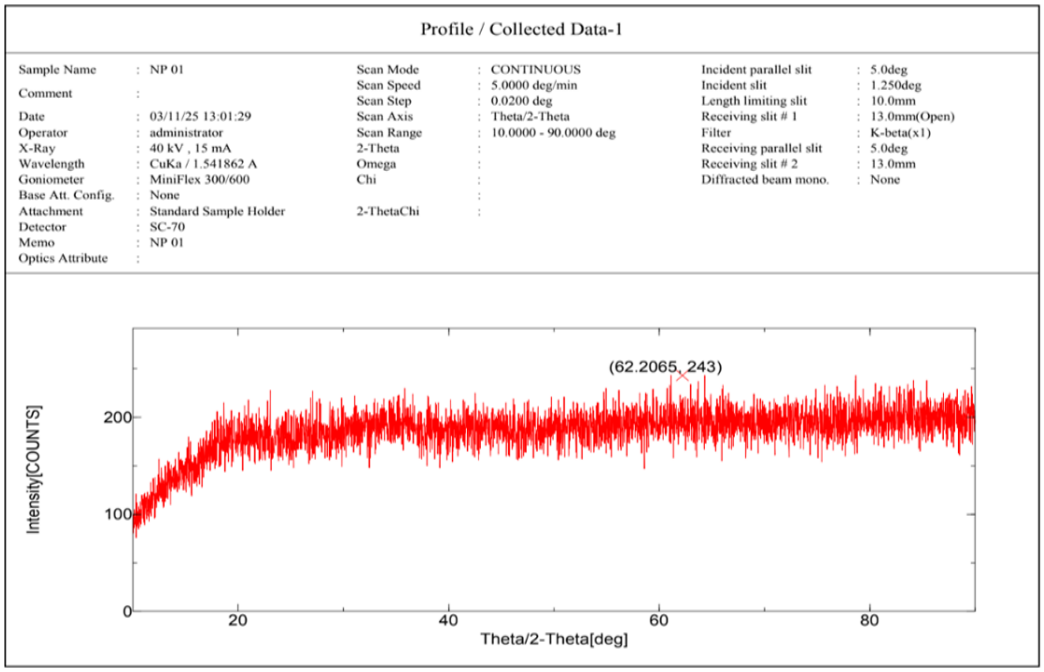


**Figure 4.** XRD pattern of green synthesized iron oxide nanoparticles

**Figure 4** displays the X-ray diffraction (XRD) pattern of the generated iron oxide nanoparticles, revealed a broad diffraction peak centered around 2θ ≈ 62.2°, which corresponds to characteristic crystallographic planes of iron oxide phases such as $Fe_3O_4$ (magnetite) or α-$Fe_2O_3$ (hematite). The pronounced broadness of this peak indicates the nanocrystalline nature of the particles—an expected outcome of green synthesis methods, where bioactive phytochemicals serve as agents that reduce and cap.

Iron oxide nanoparticle production was confirmed by the observed peak locations, which are in good accord with conventional JCPDS (Joint Committee on Powder Diffraction Standards) data for iron oxides. The broad diffraction features also suggest a particle size in the nanoscale range, estimated to be approximately 20–40 nm, consistent with the size range typically associated with biogenically synthesized nanomaterials.

*Antimicrobial Activity of $Fe_3O_4$ Nanoparticles*

a)


b)

**Figure 5.** Antibacterial activity of *C.roseus*-mediated iron oxide nanoparticles against a) *Staphylococcus aureus* b) *E. coli*.

As shown in **Figure 5**, the antimicrobial activity of the green-synthesised iron oxide nanoparticles made from *C.roseus* extract was evaluated using the agar well diffusion method against two bacterial strains: Staphylococcus aureus (Gram-positive) and Escherichia coli (Gram-negative). Clear inhibition zones surrounding the wells containing the nanoparticles indicate substantial antibacterial activity against both microbial types.

A notable zone of inhibition against *E. coli* suggests that the nanoparticles effectively compromise the integrity of Gram-negative bacterial cell membranes, possibly through oxidative stress or mechanical disruption. Similarly, a well-defined inhibition zone around the *S. aureus* culture demonstrates the nanoparticles' potent action against Gram-positive bacteria. These findings support the biogenically produced iron oxide nanoparticles' broad-spectrum antibacterial capability, probably as a consequence of the residual bioactive ingredients in the plant extract combining with their nanoscale properties.

*Zone of Inhibition Measurements*

*E. coli*: 14.7 mm (total diameter) – 6 mm (well diameter) = 8.7 mm

*S. aureus*: 15.6 mm – 6 mm = 9.6 mm

Both Gram-positive and Gram-negative microorganisms are effectively inhibited by the produced iron oxide nanoparticles, according to these observed inhibition zones. Their possible use in environmental and biological antibacterial therapies is confirmed by the results.

The current work effectively illustrates the green synthesis of iron oxide nanoparticles ($Fe_3O_4$) using leaf extract from *C.roseus*, confirming the feasibility of this sustainable and environmentally friendly method. In contrast to traditional physical and chemical procedures, which frequently call for toxic reducing agents, hazardous solvents, and significant energy inputs, green synthesis presents a viable alternative (Ahmed *et al*., 2016). The approach not only lessens the impact on the environment but also increases the biological activity of the resultant nanoparticles by using phytochemicals obtained from plants as natural reduction and stabilization agents (Potbhare *et al*., 2019).

Energy-dispersive X-ray spectroscopy (EDS) confirmed the elemental composition of the generated nanoparticles, indicating that iron and oxygen were the primary constituents. The high iron content (48.82% by weight) and corresponding oxygen levels, coupled with low error margins (2.83% and 7.59%, respectively), affirm the successful formation of iron oxide. Trace amounts of sodium and calcium likely stem from the use of NaOH during synthesis and intrinsic minerals in the plant extract, respectively. The elemental data supports the presence of an Fe–O framework, vital to the nanoparticles' antibacterial and magnetic qualities (Sharma *et al*., 2019).

Morphological analysis through scanning electron microscopy (SEM) provided valuable insight into the structural features of the nanoparticles. Images captured at varying magnifications (10.0 kx to 33.0 kx) revealed nanoscale particles with diverse morphologies—including spherical, rod-shaped, and needle-like forms—often aggregated due to magnetic dipole–dipole interactions (de Jesús Ruíz-Baltazar *et al*., 2019). The observed shape variability and surface texture reflect the influence of phytochemical capping agents from the *C. roseus* extract. This surface biofunctionalization not only stabilizes the particles but may also contribute to their biological activity. The relatively uniform size distribution further indicates effective control during synthesis.

Fourier-transform infrared spectroscopy (FTIR) provided additional confirmation of the role of plant metabolites in nanoparticle synthesis. Characteristic peaks at 612.21 $cm^{-1}$, 627.59 $cm^{-1}$, and Fe–O stretching vibrations were responsible for 650.42 $cm^{-1}$, confirming the existence of iron oxide (Yardily & Sunitha, 2019). Broad absorption bands in the 3198.99–3398.40 $cm^{-1}$ range indicated O–H stretching vibrations from hydroxyl-rich compounds such as polyphenols (Bhuiyan *et al*., 2020). Peaks between 1559.89 $cm^{-1}$ and 1597.16 $cm^{-1}$ were associated with amide groups likely derived from proteins or enzymes, while bands from 1030.61–1387.97 $cm^{-1}$ corresponded to C–O and C–H functional groups. These functional moieties confirm the dual role of plant constituents in both reducing iron salts and capping the resulting nanoparticles for improved colloidal stability (Demirezen *et al*., 2018).

X-ray diffraction (XRD) analysis substantiated the crystalline nature of the biosynthesized $Fe_3O_4$ NPs. A broad peak around $2\theta \approx 62.2°$ aligns with standard diffraction patterns for iron oxide phases such as magnetite and hematite, as per JCPDS reference data (Kanagasubbulakshmi & Kadirvelu, 2017). The peak broadening is characteristic of nanoparticles with small crystallite sizes (20–40 nm), a feature typical of green-synthesized materials due to phytochemical-mediated nucleation and growth. These findings are consistent with SEM observations and highlight the capacity of plant-based methods to regulate nanoparticle dimensions effectively (Majeed & Naji, 2018).

The ability of the generated nanoparticles to combat Gram-negative Gram-positive and Escherichia coli bacteria to assess Staphylococcus aureus, the agar well diffusion method was

employed. Zones of inhibition with corresponding measurements of 8.7 mm and 9.6 mm show strong antibacterial activity. The observed efficacy is caused by a number of mechanisms, including the generation of reactive oxygen species (ROS), the breakdown of bacterial membranes, and the disruption of intracellular constituents like proteins and nucleic acids (Prabhu *et al*., 2015). Moreover, bioactive compounds from the plant extract may synergistically enhance the antimicrobial effects by facilitating better interaction between nanoparticles and bacterial cells. These results align with previous reports highlighting the superior biological activity of plant-mediated nanoparticles, confirming their broad-spectrum antibacterial potential. Thus, green-synthesized $Fe_3O_4$ nanoparticles offer a dual advantage—environmental sustainability and enhanced functional performance (Gouyau *et al*., 2021).

## Conclusion

This work uses an aqueous extract of the phytochemical-rich medicinal plant *C.roseus* to create iron oxide nanoparticles ($Fe_3O_4$) in a sustainable and environmentally friendly manner. This environmentally friendly method provides a cost-effective synthesis pathway while avoiding hazardous ingredients and adhering to green chemistry principles. The generation of nanoscale, spherical, and crystalline $Fe_3O_4$ nanoparticles with surface functional groups produced from the plant extract was verified by characterization (XRD, FTIR, SEM, and EDX). It is probable that phytochemicals such terpenoids, alkaloids, flavonoids, and phenolics served as both stabilizing and reducing agents, improving the functioning and stability of nanoparticles. The generated $Fe_3O_4$ nanoparticles showed strong antibacterial effect against both Gram-positive and Gram-negative bacteria. High surface area, magnetic characteristics, and the formation of reactive oxygen species (ROS) disrupt bacterial membranes and cellular processes. Further enhancing antibacterial activity was the synergistic action of biomolecules originating from plants. These results highlight the possibility of using *C.roseus* mediated $Fe_3O_4$ nanoparticlesin pharmacological, environmental, and biological applications. Future studies should explore in vivo toxicity, optimal nanoparticle concentration and size, and detailed mechanisms of action. Extending the research to include fungal and drug-resistant strains could further validate their therapeutic value and support sustainable solutions to antibiotic resistance and environmental contamination.

**Acknowledgments:** None

**Conflict of interest:** None

**Financial support:** None

**Ethics statement:** None

## References

Abdel-Hadi, B., & Abdel-Fattah, S. R. (2022). Clinical pharmacist intervention in appendectomy - dexmedetomidine as an adjunct therapy. *Journal of Advanced Pharmacy Education and Research, 12*(2), 1–5. doi:10.51847/AYOZXtLMrj

Abo-zeid, Y., & Williams, G. R. (2020). The potential anti-infective applications of metal oxide nanoparticles: a systematic review. *Wiley Interdisciplinary Reviews: Nanomedicine and Nanobiotechnology, 12*(2), e1592.

Ahmed, S., Ahmad, M., Swami, B. L., & Ikram, S. (2016). Green synthesis of silver nanoparticles using *Azadirachta indica* aqueous leaf extract. *Journal of Radiation Research and Applied Sciences, 9*(1), 1–7.

Akhmedov, M. Y., Akhmedova, A. T., Demirov, Z. A., Demirov, M. A., Magomedova, M. G., Magomedov, K. N., Abduragimova, M. A., & Kitalaev, K. Z. (2024). Fluorescent diagnostics of microscopic damage to tooth enamel using an innovative mixture of silver nanoparticles. *Annals of Dental Specialty, 12*(3), 48–52. doi:10.51847/iWg8hdqiSl

Alamu, G. A., Ayanlola, P. S., Babalola, K. K., Adedokun, O., Sanusi, Y. K., & Fajinmi, G. R. (2024). Green synthesis and characterizations of magnetic iron oxide nanoparticles using *Moringa oleifera* extract for improved performance in dye-sensitized solar cell. *Chemical Physics Impact, 8,* 100542.

Alexeree, S. M., Abou-Seri, H. M., El-Din, H. E. S., Youssef, D., & Ramadan, M. A. (2024). Green synthesis of silver and iron oxide nanoparticles mediated photothermal effects on *Blastocystis hominis*. *Lasers in Medical Science, 39*(1), 43.

Alharith, D. N., Mansi, I. T., Abdulmotalib, Y., Amous, H., Aljulban, T., Aiban, H. M. A., & Haffar, S. M. (2023). Radiographic evaluation of periapical healing rates between bio-ceramic sealer and AH+ sealer: a retrospective study. *Annals of Dental Specialty, 11*(2), 124–128. doi:10.51847/rTpmLOU0gT

Alhazmi, R. A., Khayat, S. K., Albakri, M. H., Alruwaili, W. S., Bayazed, H. A., Almubarak, S. A., Albahrani, A. A., Alshahrani, A. A., Alharkan, A. A., Alreqei, H. M., et al. (2022). An overview on the assessment and management of polycystic ovarian syndrome. *World Journal of Environmental Biosciences, 11*(1), 17–23. doi:10.51847/Yaaa2745ZY

Aljerf, L., & Nadra, R. (2019). Developed greener method based on MW implementation in manufacturing CNFs. *International Journal of Nanomanufacturing, 15*(3), 269–289.

Almohmmadi, G. T., Bamagos, M. J., Al-Rashdi, Y. J. R., Alotaibi, N. S., Alkiyadi, A. A., Alzahrani, A. M., Alotaibi, H. R., Alenazi, N. F. N., Alqissom, M. A., & Alrefaei, K. I. (2022). Literature review on polycythemia vera diagnostic and management approach. *World Journal of Environmental Biosciences, 11*(1), 9–12. doi:10.51847/ipOt4R1qlz

Almuhanna, M. A., Alanazi, M. H., Ghamdi, R. N. A., Alwayli, N. S., Alghamdi, I. S. G., Qari, A. A., Alzahid, A. A., Alharbi, F. F., Alwagdani, N. M. A., & Alharthi, S. A. (2022). Tachycardia evaluation and its management approach, literature review. *World Journal of Environmental Biosciences, 11*(1), 4–8. doi:10.51847/7maH6sWjQy

Alqurashi, A. M. A., Jawmin, S. A. H., Althobaiti, T. A. A., Aladwani, M. N. M. F. A., Almuebid, A. M. E., Alharbi, J. F. A., Zarei, M. A., Ghaseb, L. S. A. A., Nawwab, W. K., Zamzamy, N. A., et al. (2022). An overview on nasal

polyps' diagnosis and management approach. *World Journal of Environmental Biosciences, 11*(1), 13–16. doi:10.51847/gde2ofOvaO

Alsayed, M. A., Alhassan, O. M. A., Alzahrany, A. M., Mutanbak, H. I. M., Alamoudi, A. A., Eid, S. M., Shaikh, D. T., Alhumaid, Z. A., Alshafai, A. S., & Zarei, M. A. H. (2022). An overview on lumbar disc herniation on surgical management approach. *World Journal of Environmental Biosciences, 11*(1), 24–29. doi:10.51847/OJ2dQINEwx

Asfahani, A. (2022). The effect of organizational citizenship behavior on counterproductive work behavior: A moderated mediation model. *Journal of Organizational Behavior Research, 7*(2), 143–160. doi:10.51847/sRtILGuTSd

Bhuiyan, M. S. H., Miah, M. Y., Paul, S. C., Aka, T. D., Saha, O., Rahaman, M. M., Sharif, M. J. I., Habiba, O., & Ashaduzzaman, M. (2020). Green synthesis of iron oxide nanoparticle using *Carica papaya* leaf extract: application for photocatalytic degradation of remazol yellow RR dye and antibacterial activity. *Heliyon*, *6*(8), e04603. doi:10.1016/j.heliyon.2020.e04603

Buarki, F., AbuHassan, H., Al Hannan, F., & Henari, F. Z. (2022). Green synthesis of iron oxide nanoparticles using *Hibiscus rosa sinensis* flowers and their antibacterial activity. *Journal of Nanotechnology, 2022*(1), 5474645.

Chinnasamy, R., Chinnaperumal, K., Cherian, T., Thamilchelvan, K., Govindasamy, B., Vetrivel, C., Perumal, V., Willie, P., & Krutmuang, P. (2024). Eco-friendly phytofabrication of silver nanoparticles using aqueous extract of *Aristolochia bracteolata* Lam: Its antioxidant potential, antibacterial activities against clinical pathogens and malarial larvicidal effects. *Biomass Conversion and Biorefinery, 14*(22), 28051–28066.

Dadfar, S. M., Roemhild, K., Drude, N. I., von Stillfried, S., Knüchel, R., Kiessling, F., & Lammers, T. (2019). Iron oxide nanoparticles: Diagnostic, therapeutic and theranostic applications. *Advanced Drug Delivery Reviews, 138,* 302–325.

de Jesús Ruíz-Baltazar, Á., Reyes-López, S. Y., de Lourdes Mondragón-Sánchez, M., Robles-Cortés, A. I., & Pérez, R. (2019). Eco-friendly synthesis of Fe3O4 nanoparticles: Evaluation of their catalytic activity in methylene blue degradation by kinetic adsorption models. *Results in Physics, 12,* 989–995.

Demirezen, D. A., Yilmaz, D., & Yılmaz, Ş. (2018). Green synthesis and characterization of iron nanoparticles using *Aesculus hippocastanum* seed extract. *International Journal of Advanced Science Engineering and Technology, 6,* 2321–8991.

Figueroa-Valverde, L., Marcela, R., Alvarez-Ramirez, M., Lopez-Ramos, M., Mateu-Armand, V., & Emilio, A. (2024). Statistical data from 1979 to 2022 on prostate cancer in populations of northern and central Mexico. *Bulletin of Pioneering Researches of Medical and Clinical Science, 3*(1), 24–30. doi:10.51847/snclnafVdg

Gajalakshmi, S., Vijayalakshmi, S., & Devi, R. V. (2013). Pharmacological activities of *Catharanthus roseus*: a perspective review. *International Journal of Pharma and Bio Sciences, 4*(2), 431–439.

Gavamukulya, Y., Abou-Elella, F., Wamunyokoli, F., & AEl-Shemy, H. (2014). Phytochemical screening, antioxidant activity and in vitro anticancer potential of ethanolic and water leaves extracts of *Annona muricata* (Graviola). *Asian Pacific Journal of Tropical Medicine, 7,* S355–S363.

Gouyau, J., Duval, R. E., Boudier, A., & Lamouroux, E. (2021). Investigation of nanoparticle metallic core antibacterial activity: Gold and silver nanoparticles against *Escherichia coli* and *Staphylococcus aureus*. *International Journal of Molecular Sciences, 22*(4), 1905.

İlaslan, E., Adıbelli, D., Teskereci, G., & Cura, Ş. Ü. (2023). Studying the impact of clinical decision-making and critical thinking on the quality of nursing care. *Journal of Integrative Nursing and Palliative Care, 4*, 23–29. doi:10.51847/fsTLiDadY3

İlhan, N., Telli, S., Temel, B., & Aştı, T. (2022). Investigating the sexual satisfaction mediating role in the relationship between health literacy and self-care of men with diabetes and women's marital satisfaction. *Journal of Integrative Nursing and Palliative Care, 3*, 19–25. doi:10.51847/sFjL3OLpqg

Kanagasubbulakshmi, S., & Kadirvelu, K. (2017). Green synthesis of iron oxide nanoparticles using *Lagenaria siceraria* and evaluation of its antimicrobial activity. *Defence Life Science Journal, 2*(4), 422–427.

Kariri, H. D. H., Radwan, O. A., Somaili, H. E., Mansour, M. E. I., Mathkoor, S. A., & Gohal, K. M. M. (2022). The relationship of psychological capital to psychological empowerment among female workers at leadership positions. *Journal of Organizational Behavior Research, 7*(2), 243–258. doi:10.51847/7IGwvNc6i0

Kauser, S., Morrissey, H., & Ball, P. (2022). England local community pharmacists opinions on independent prescribing training. *Journal of Advanced Pharmacy Education and Research, 12*(1), 30–37. doi:10.51847/PaNZ94aVtA

Kwatra, D., Venugopal, A., & Anant, S. (2024). Studying the efficacy of tolmetin radiosensitizing effect in radiotherapy treatment on human clonal cancer cells. *Bulletin of Pioneering Researches of Medical and Clinical Science, 3*(2), 22–28. doi:10.51847/Uuhjk0fMC8

Ma, M., Zhang, Y., Guo, Z., & Gu, N. (2013). Facile synthesis of ultrathin magnetic iron oxide nanoplates by Schikorr reaction. *Nanoscale Research Letters, 8*(1), 16.

Majeed, N. S., & Naji, D. M. (2018). Synthesis and characterization of iron oxide nanoparticles by open vessel ageing process. *Iraqi Journal of Chemical and Petroleum Engineering, 19*(2), 27–31.

Maneea, A. S. B., Alqahtani, A. D., Alhazzaa, A. K., Albalawi, A. O., Alotaibi, A. K., & Alanazi, T. F. (2023). Microbiological effect of various concentrations of sodium hypochlorite (NaOCL) during endodontic treatment: a systematic review. *Annals of Dental Specialty, 11*(1), 95–101. doi:10.51847/7CZTguksH9

Maskurova, Y. V., Kokoev, V. A., Gusengadzhiev, K. A., Megrikyan, A. A., Alieva, K. M., & Serov, N. G. (2023). Structural and mechanical assessment of dental implants based on TiO2 and ZrO2. *Annals of Dental Specialty, 11*(2),

94–98. doi:10.51847/gFHZM9fdj8

Moorthi, P. V., Balasubramanian, C., & Mohan, S. (2015). An improved insecticidal activity of silver nanoparticle synthesized by using *Sargassum muticum*. *Applied Biochemistry and Biotechnology, 175*(1), 135–140.

Nakagawa, N., Odanaka, K., Ohara, H., Ito, T., Kisara, S., & Ito, K. (2022). Effect of smartphone location on pharmacy students' attention and working memory. *Journal of Advanced Pharmacy Education and Research, 12*(2), 84–90. doi:10.51847/7tgmB6sV8i

Nguyen, T. H., Nguyen, V. H., Vo, H. H., Le, N. T., Nguyen, T. T. P., & Vo, H. K. (2022a). Emotional intelligence and teamwork results of Vietnamese students. *Journal of Organizational Behavior Research, 7*(2), 171–187. doi:10.51847/uVJ1OoEjXq

Nguyen, T. P. L., Nguyen, T. T., Nguyen, T. D., & Nguyen, T. V. H. (2022b). Psychological empowerment and employee creativity in Vietnam telecommunication enterprises: the mediating role of intrinsic work motivation. *Journal of Organizational Behavior Research, 7*(2), 132–142. doi:10.51847/0xkWbKBEHE

Nnadozie, E. C., & Ajibade, P. A. (2020). Green synthesis and characterization of magnetite (Fe3O4) nanoparticles using *Chromolaena odorata* root extract for smart nanocomposite. *Materials Letters, 263,* 127145.

Patra, J. K., & Baek, K. H. (2014). Green nanobiotechnology: Factors affecting synthesis and characterization techniques. *Journal of Nanomaterials, 2014*(1), 417305.

Pham, H. N. T., Vuong, Q. V., Bowyer, M. C., & Scarlett, C. J. (2020). Phytochemicals derived from *Catharanthus roseus* and their health benefits. *Technologies, 8*(4), 80.

Pirsaheb, M., Gholami, T., Seifi, H., Dawi, E. A., Said, E. A., Hamoody, A. M., Altimari, U. S., & Salavati-Niasari, M. (2024). Green synthesis of nanomaterials by using plant extracts as reducing and capping agents. *Environmental Science and Pollution Research International*, *31*(17), 24768–24787. doi:10.1007/s11356-024-32983-x

Potbhare, A. K., Chaudhary, R. G., Chouke, P. B., Yerpude, S., Mondal, A., Sonkusare, V. N., Rai, A. R., & Juneja, H. D. (2019). Phytosynthesis of nearly monodisperse CuO nanospheres using Phyllanthus reticulatus/Conyza bonariensis and its antioxidant/antibacterial assays. *Materials Science & Engineering. C, Materials for Biological Applications*, *99*, 783–793. doi:10.1016/j.msec.2019.02.010

Prabhu, Y. T., Rao, K. V., Kumari, B. S., Kumar, V. S. S., & Pavani, T. (2015). Synthesis of $Fe_3O_4$ nanoparticles and its antibacterial application. *International Nano Letters, 5*(2), 85–92.

Rahmani, R., Gharanfoli, M., Gholamin, M., Darroudi, M., Chamani, J., Sadri, K., & Hashemzadeh, A. (2020). Plant-mediated synthesis of superparamagnetic iron oxide nanoparticles (SPIONs) using aloe vera and flaxseed extracts and evaluation of their cellular toxicities. *Ceramics International, 46*(3), 3051–3058.

Seifi, S., & Masoum, S. (2020). Synthesis of $Co_9S_8$@N, S co-doped porous carbon core–shell nanocomposite with highly coulombic efficiency in electrochemical hydrogen storage application. *Journal of The Electrochemical Society, 167*(11), 110539.

Sharma, D., Kanchi, S., & Bisetty, K. (2019). Biogenic synthesis of nanoparticles: A review. *Arabian Journal of Chemistry, 12*(8), 3576–3600.

Shaykhaeva, K. S., Mamaeva, M. B., Magomadova, A. Z., Kokaeva, D. R., Mishchenko, O. A., Arselgova, D. A., Askarova, U. R., & Abakumova, E. I. (2024). Assessment of morpho-structural changes at increased erasability of teeth with atomic force microscopy. *Annals of Dental Specialty, 12*(3), 42–47. doi:10.51847/Ri6GsKx4YC

Singh, P., Kim, Y. J., Zhang, D., & Yang, D. C. (2016). Biological synthesis of nanoparticles from plants and microorganisms. *Trends in Biotechnology, 34*(7), 588–599.

Sirelkhatim, A., Mahmud, S., Seeni, A., Kaus, N. H. M., Ann, L. C., Bakhori, S. K. M., Hasan, H., & Mohamad, D. (2015). Review on Zinc Oxide Nanoparticles: Antibacterial Activity and Toxicity Mechanism. *Nano-Micro Letters*, *7*(3), 219–242. doi:10.1007/s40820-015-0040-x

Soboleva, M. S., Loskutova, E. E., & Kosova, I. V. (2022). Pharmacoepidemiological study of the use of e-pharmacies by the population. *Journal of Advanced Pharmacy Education and Research, 12*(3), 36–43. doi:10.51847/osvixvsOlX

Üzüm, B., Özkan, O. S., & Çakan, S. (2022). Moral disengagement, organizational broken window, person-organization fit as an antecedent: Machiavellian leadership. *Journal of Organizational Behavior Research, 7*(1), 29–41. doi:10.51847/54QfKceM1p

Venkateswarlu, S., Kumar, B. N., Prasad, C. H., Venkateswarlu, P., & Jyothi, N. V. V. (2014). Bio-inspired green synthesis of $Fe_3O_4$ spherical magnetic nanoparticles using *Syzygium cumini* seed extract. *Physica B: Condensed Matter, 449*, 67–71.

Vitta, Y., Figueroa, M., Calderon, M., & Ciangherotti, C. (2020). Synthesis of iron nanoparticles from aqueous extract of *Eucalyptus robusta* Sm and evaluation of antioxidant and antimicrobial activity. *Materials Science for Energy Technologies, 3*, 97–103.

Xuan, E. Y. H., Razak, N. F. A., Ali, A. M., & Said, M. M. (2022). Evaluation of knowledge, attitudes, and perceptions on halal pharmaceuticals among pharmacy students from Malaysian private universities. *Journal of Advanced Pharmacy Education and Research, 12*(1), 84–90. doi:10.51847/D3bNfyJZ6t

Yardily, A., & Sunitha, N. (2019). Green synthesis of iron nanoparticles using hibiscus leaf extract, characterization, antimicrobial activity. *International Journal of Scientific Research and Review, 8*(7).

Yassin, M. T., Al-Otibi, F. O., & Al-Askar, A. A. (2024). Green synthesis, characterization and antimicrobial activity of iron oxide nanoparticles with tigecycline against multidrug resistant bacterial strains. *Journal of King Saud University-Science, 36*(4), 103131.

Yoong, S. Q., Wang, W., Seah, A. C. W., Kumar, N., Gan, J. O. N., Schmidt, L. T., Lin, Y., & Zhang, H. (2022). Study of the self-care status and factors related to it in heart failure patients. *Journal of Integrative Nursing and Palliative Care,*

*3*, 31–35. doi:10.51847/Lqz1ms7fB8

Zhan, Y., Hu, H., Yu, Y., Chen, C., Zhang, J., Jarnda, K. V., & Ding, P. (2024). Therapeutic strategies for drug-resistant *Pseudomonas aeruginosa*: metal and metal oxide nanoparticles. *Journal of Biomedical Materials Research Part A, 112*(9), 1343–1363.